Understanding Ignition Mechanisms and Improving Temperature Boundary Condition for Lithium-Ion Battery Vent Gas Simulations

N.A.C.J.D. Senarathna, M-A. Bérubé, P. Versailles, E. Robert, and B. Savard
Department of Mechanical Engineering, Polytechnique Montréal
Montréal
QC, Canada

January 27, 2025

1 Introduction

The demand for lithium-ion (Li-ion) cells has surged in recent years, particularly in the transportation sector, due to their high energy density and long cycle life. However, these batteries carry an inherent risk of thermal runaway (TR), during which they can eject large amounts of flammable and toxic gases alongside incandescent particles, creating multiphase jets with flame temperatures exceeding 2000 K [1, 2]. Accurate modeling of this vented gas combustion is critical for designing effective mitigation strategies, especially since the failure of a single cell can propagate through entire battery modules containing thousands of cells in electric vehicles.

Despite extensive research, the ignition mechanism of vent gases remains unclear. Two primary hypotheses —auto-ignition (AI) of the hot vent gas-air mixture [3, 4] and ignition triggered by incandescent particles [5, 6]—have been proposed, but direct evidence supporting either is lacking. For instance, Kim et al. [6] observed hot particles in the proximity of ignition sites and proposed that these particles might serve as ignition sources. However, no ignition event clearly initiated by these particles was observed. Similarly, Nilsson et al. [3] report low AI delay times for certain vent gas mixtures, suggesting the possibility of AI, though they acknowledged the importance of considering the vent gas residence time—a factor not considered in their study. Hence, it remains unclear whether the flammable mixture, formed as hot vent gas mixes with ambient air, can self-ignite or if external heat sources, such as ejected incandescent particles, are needed to initiate ignition.

Moreover, current studies characterizing TR typically report average vent gas compositions and cell wall temperatures rather than instantaneous compositions and actual vent gas temperatures [1]. As a result, computational fluid dynamics (CFD) models for vent gas combustion generally rely on experimental cell wall temperatures as a proxy for vent gas temperature [7]. However, reported large temperature differences between the jelly roll and the cell surface (487 °C) raise doubts about whether the wall temperature accurately represents the vent gas, which could have significant implications for CFD studies [5].

Correspondence to: chathura-senarathna.nammuni-arachchilage@polymtl.ca

The present study aims to clarify the ignition mechanisms of Li-ion cell vent gases and determine whether the cell wall temperature corresponds to their temperature. The high-speed imaging techniques and the numerical methods used to scrutinize the ignition mechanism are detailed in Section 2. Section 3 presents findings on ignition mechanisms and vent gas temperatures, while Section 4 concludes with key insights and implications.

2 Methodology

TR is deliberately triggered in five Samsung 18650-25R NMC cells in separate tests via controlled heating, and the resulting venting events are recorded using a high-speed camera. To assess whether the incandescent particles play a role in igniting the vent gases, the ignition kernels (*i.e.*, the first observable instance of a flame front) are isolated and visually analyzed. The possibility of AI is evaluated by comparing the order of magnitude of experimentally observed AI delays with those calculated numerically; if the computed delays align with the observed values, it suggests that the vent gas properties are conducive to AI, making its occurrence likely. Additionally, the vent gas temperature is inferred by measuring the cell cap temperature using two-color pyrometry (2-CP); the cap in direct contact with the vented gas is presumed to provide a more accurate estimate than the cell wall. Detailed experimental procedures and the approach for calculating ignition delays are presented in the following subsections.

2.1 Experimental procedure

As illustrated in Fig. 1, for each of the five tests, a fully charged Samsung 18650-25R cell (2.5 Ah capacity, 3.6 V nominal voltage) is tightly placed inside a copper tube wrapped into two heating cables (McMaster 3641K22, 100 W) connected in parallel to a solid-state relay (Omega SSRL240DC25). Using the signal from a thermocouple taped to the cell wall, a PID control system developed in LabVIEW regulates the power supplied to the heating cables. The experimental setup is placed inside a blast box to safely contain the blast and vent any toxic gases without altering the flow field. A Photron high-speed camera (FASTCAM Mini AX200 900K), operated at 10,000 fps and 1/18,000 s exposure time, is used to record the event, with its focal plane carefully aligned to experimentally estimate the ignition delay from the velocity of the particles. Additionally, a Telops multispectral IR camera (MS-M350) is focused on the cell cap to measure temperature via 2-CP. The cap temperature is calculated using the in-band radiance ratio between two spectrally close filters (filters 7 and 8) exposed for 100 µs, and comparing it to theoretical values derived from Planck's law, with the average temperature obtained over a circular region at the cap center.

With the experimental setup in place, the cell heating at a controlled rate of 10 °C/min and high-speed camera recording are started. Upon reaching 55 °C, the cell temperature is stabilized for 10 minutes, following the RTCA DO-311A testing protocol. Heating then resumes at the same rate until the first gas venting occurs at which point imaging with the multispectral camera begins to measure the cell cap temperature. If TR does not spontaneously occur after the first venting, which is indicated by a monotonic temperature decrease, heating restarts (10 °C/min) at 120 °C and stops at the second venting.

2.2 Experimental and numerical ignition delay evaluation

The ignition delay (*i.e.*, the residence time of the gas prior to ignition) can be estimated by integrating the reciprocal of time-resolved gas velocities along the trajectory. However, precise time- and space-resolved measurements of gas velocity pose significant experimental challenges, as they require non-intrusive techniques that do not inadvertently trigger ignition. Nevertheless, following the suggestion

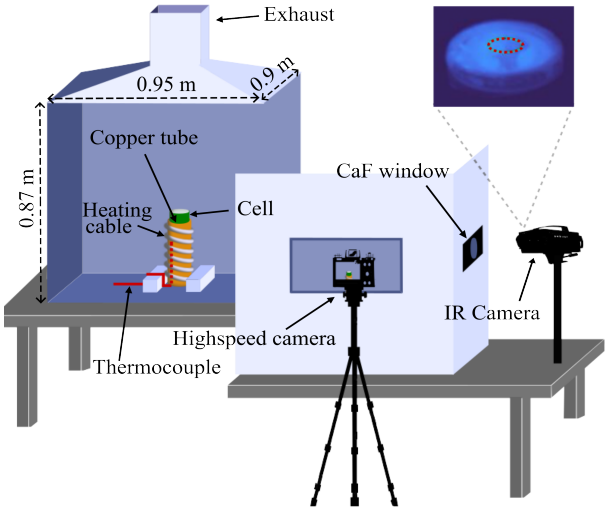

Figure 1: Exploded view of the experimental setup including the IR image of the cell cap as captured by filter 7 (not to scale).

of Fedoryshyna et al. [8], which states that particle velocities can be up to five times slower than gas velocities, the ignition delay can be approximated (τ_{est}) within one order of magnitude by tracking the trajectories of particles traveling near the ignition location and using mean particle velocities $\overline{V_{\text{t}}^{\text{p}}}$ as a proxy:

$$\tau_{\text{est}} \simeq \frac{s_{\text{ig}} - s_0}{\overline{V_{\text{t}}^{\text{p}}}},$$

where s_0 and s_{ig} denote the distances along the particle trajectory corresponding to the vent exit and the ignition location, respectively. Particle tracking is carried out using an in-house MATLAB algorithm, which employs a Kalman filter to predict the location of a particle in the subsequent frame based on upstream data. The James Munkres variation of the Hungarian algorithm is then used to associate particles in the next frame with these predictions. After tracing the trajectories, particle velocities are computed using a central difference scheme. Both velocities and distances are calibrated using a dotted grid imaged prior to the TR event.

To determine the numerical ignition delay, the constant pressure reactor module in the Cantera software package is employed [9]. When vented gases are ejected, they form a turbulent jet that entrains ambient air, resulting in a range of mixture fractions—the normalized mass ratio of fuel in an air-fuel mixture—spanning from 0 (pure air) to 1 (pure fuel) across the jet. For Li-ion cell jets, as cold air mixes with hot vent gases, the local mixture temperature increases with the mixture fraction. To account for these dynamics, adiabatic, homogeneous reactor simulations are conducted across the full range of vented gas/air mixtures, incorporating the corresponding mixture enthalpy. The temperature rise caused by spontaneous exothermic reactions is predicted, and the AI delay is defined as the time taken for the rate of temperature increase to reach its maximum. Vent gas composition and temperature data from Golubkov et al. [1] (30.8% H_2, 41.2% CO_2, 13% CO, 6.8% CH_4, and 8.2% C_2H_4, and cell wall temperature of 950 K), are used to evaluate AI under nominal conditions, with parametric studies in the temperature space conducted to identify conditions that favor AI.

3 Results and Discussion

This section examines ignition mechanisms of vent gases and explores the potential for vent gas temperatures exceeding cell wall values, with implications for AI and CFD models.

3.1 Ignition mechanisms

To investigate the ignition mechanisms, ignition kernels, visually distinct regions that grow in size and intensity over time, were first identified (see Fig. 2). Sequences of images capturing kernel formation, and subsequent flame front development until extinction or exit from the field of view were then isolated and cropped to focus on the ignition spot. Finally, MATLAB's *localcontrast* algorithm was applied to enhance contrast, facilitating the detection of even faint particles potentially involved in the ignition process. Fig. 2 illustrates two such sequences of ignition kernels. Sequence 1 (Fig. 2(a)-(d)) illustrate a kernel initiated by a particle. In Fig. 2(a), the particle involved in the ignition, visible as a bright white blob boxed in green, is shown 0.3 ms prior to ignition with a zoomed-in view for clarity. As illustrated in Fig. 2(b), this particle initiates an ignition kernel. The particle then exits the ignition spot, and initiates another consecutive ignition kernel (Fig. 2(c)) 0.3 ms after the first. Finally, the two kernels merge, creating a propagating flame front, as depicted in Fig. 2(d). When high-temperature particles travel through the highly stratified mixture resulting from the mixing of hot vent gases and ambient air they transfer heat to the surrounding gas through convection, increasing the local gas temperature and triggering ignition. Furthermore, multiple instances of particle-induced ignition kernels were identified, providing clear evidence that particles could contribute to the ignition of Li-ion cell vent gases.

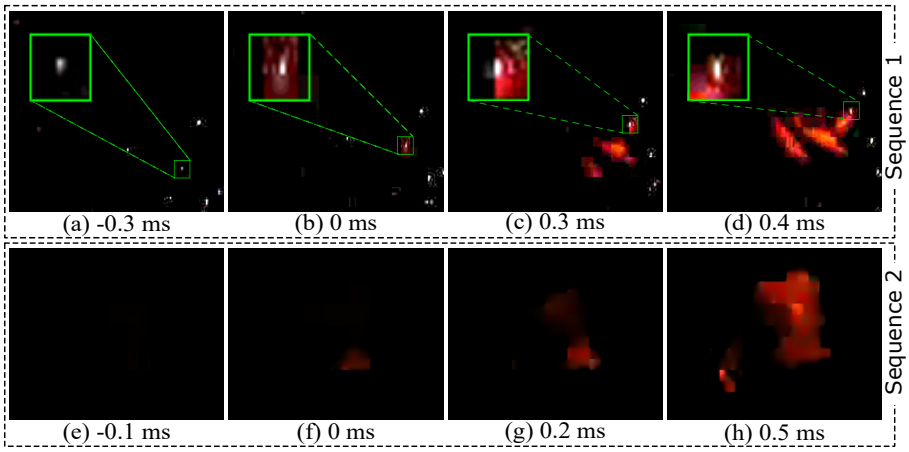

Figure 2: Two high-speed image sequences recorded at 10,000 fps illustrating ignition mechanisms: (a)-(d) shows two successive ignition kernels induced from the same particle, while (e)-(f) depicts a kernel not assisted by any detectable particle

As shown in Fig. 2(e)-(f) (Sequence 2), ignition can also occur without the assistance of detectable particles. Fig. 2(e), taken 0.1 ms before ignition and enhanced using MATLAB's *localcontrast*, confirms the absence of even dim particles at the site where an ignition kernel subsequently forms (Fig. 2(f)). The kernel then propagates downstream (Figs. 2(g)-(h)) and, eventually stabilizes as an anchored jet flame. The high temperature of the vented gas coupled with the occurrence of ignition sites independent of detectable particles, strongly indicates that self-ignition of the combustible mixture can occur without external triggers, which is further investigated in Section 3.2.

3.2 Likelihood of higher vent gas temperatures and AI

As described in the methodology section, the likelihood of AI is assessed by comparing the order of magnitude of experimentally observed ignition delays with numerically predicted values. Six ignition kernels not assisted by particles were selected from five tests, while also ensuring the presence of particles upstream and downstream of the ignition spots to enable reliable estimation of ignition delays, as detailed in Section 2.2. The distances to the ignition locations from the vent, average particle velocities, and the ignition delays for these kernels are presented in Table 1, indicating that the experimentally observed ignition delays consistently fall within the order of 1 ms or less.

Table 1: Ignition delay time of ignition kernels without particle assistance.

Ignition Kernel	Distance (m)	Average Velocity (m/s)	Ignition Delay (ms)
1	0.010	32.5	0.307
2	0.075	21.3	3.521
3	0.189	64.5	2.930
4	0.119	42.4	2.800
5	0.080	25.3	3.169
6	0.076	13.9	5.453

Fig. 3(a) shows the numerically predicted AI delay for air-vent gas mixtures, at nominal properties reported in the literature, across a range of mixture fractions from pure fuel to lean mixtures. The results indicate an exponential increase in AI delay with decreasing mixture fraction due to the adiabatic mixing of hot vent gas with ambient air; decreasing the mixture fraction results in lower temperatures, and AI is fundamentally known to exhibit exponential sensitivity to temperature. Consequently, the most reactive mixture, the one with the shortest ignition delay, is found near the pure fuel side. Notably, the minimum predicted AI delay under nominal conditions is 190 ms, two orders of magnitude larger than the experimentally observed values, strongly suggesting that AI is unlikely under these conditions.

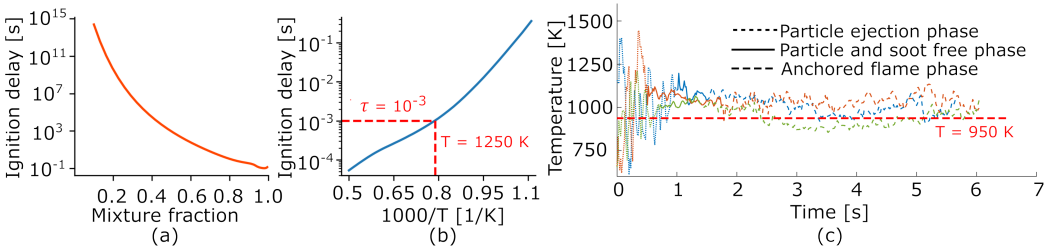

Figure 3: (a) AI delay for vent gas from NMC cells across mixture fractions at nominal composition and cell wall temperature, (b) AI delay for the most reactive mixture as a function of fuel temperature, and (c) average cell cap temperature measured using 2-CP.

This discrepancy raises the question whether the commonly reported cell wall temperature (950 K) accurately reflects the vent gas temperature or, otherwise, if the actual gas temperature is significantly higher making AI probable. A sensitivity analysis of AI delay on temperature, therefore, was conducted. Fig. 3(b) presents the minimum ignition delay as a function of the reciprocal of the vent gas temperature. It reveals that ignition delays on the order of 1 ms, consistent with experimental observations, are predicted at a vent gas temperature of ∼1250 K. Although this temperature is substantially higher than the cell wall, 2-CP measurements on the cell cap provide evidence that such elevated vent gas temperatures are achievable (see Fig. 3 (c)). Due to particle ejection obscuring the line of sight to the cell cap in the early stages of TR (indicated by dotted lines) and soot from the anchored flame in later stages (indicated by dashed lines), reliable temperature readings (represented by solid lines) are only available for a few

milliseconds in-between. Nevertheless, these measurements reveal that cell cap temperatures can reach up to 1200 K, aligning with the numerically predicted temperature range required to enable AI.

4 Conclusion

This study, combining numerical and experimental approaches, provides insights into the ignition mechanisms of Li-ion cell vent gases. High-speed imaging of ignition kernels revealed that vent gases can ignite upon contact with incandescent particles and, in some cases, without the assistance of detectable particles. However, a comparison of experimentally and numerically obtained ignition delays indicates that self-ignition of vent gases under the nominal conditions reported in the literature is highly unlikely. Nevertheless, two-color pyrometry measurements of the cell cap demonstrated temperatures reaching up to 1200 K, significantly exceeding the cell wall temperatures commonly reported in the literature. A sensitivity analysis showed that such elevated temperature makes AI in the gas phase possible. These findings demonstrate that vent gases are significantly warmer than cell wall, which should not be used as a proxy for vent gas temperatures in CFD simulations.

References

[1] Golubkov AW, Fuchs D, Wagner J, Wiltsche H, Stangl C, Fauler G, Voitic G, Thaler A, Hacker V. (2014). Thermal-runaway experiments on consumer Li-ion batteries with metal-oxide and olivin-type cathodes. RSC Adv. 4(7): 3633-3642.

[2] Kim J, Mallarapu A, Finegan DP, Santhanagopalan S. (2021). Modeling cell venting and gas-phase reactions in 18650 lithium-ion batteries during thermal runaway. J. Power Sources 489: 229496.

[3] Nilsson EJK, Brackmann C, Ahlberg Tidblad A. (2023). Evaluation of combustion properties of vent gases from Li-ion batteries. J. Power Sources 585: 233638.

[4] Mathieu O, Grégoire CM, Turner MA, Mohr DJ, Alturaifi SA, Thomas JC, Petersen EL. (2022). Experimental investigation of the combustion properties of an average thermal runaway gas mixture from Li-ion batteries. Energy Fuels 36(6): 3247-3258.

[5] Wang H, Xu H, Zhao Z, Wang Q, Jin C, Li Y, Sheng J, Li K, Du Z, Xu C. (2022). An experimental analysis on thermal runaway and its propagation in Cell-to-Pack lithium-ion batteries. Appl. Therm. Eng. 211: 118-418.

[6] Kim D, Sim I, Shin J, Park S. (2023). Analysis of thermal runaway in pouch-type lithium-ion batteries using particle image velocimetry. Int. J. Energy Res. 2023(1): 5568642.

[7] Cellier A, Duchaine F, Poinsot T, Okyay G, Leyko M, Pallud M. (2023). An analytically reduced chemistry scheme for large eddy simulation of lithium-ion battery fires. Combust. Flame 250: 112648.

[8] Fedoryshyna Y, Schaeffler S, Soellner J, Gillich EI, Jossen A. (2024). Quantification of venting behavior of cylindrical lithium-ion and sodium-ion batteries during thermal runaway. J. Power Sources 615: 235064.

[9] Goodwin DG, Moffat HK, Schoegl I, Speth RL, Weber BW. (2023). Cantera: An object-oriented software toolkit for chemical kinetics, thermodynamics, and transport processes. Version 3.0.0. Available at: https://www.cantera.org. doi: 10.5281/zenodo.8137090.